Biogeosciences Discuss., https://doi.org/10.5194/bg-2018-294
Manuscript under review for journal Biogeosciences
Discussion started: 13 July 2018

Carbon Flux Explorer Optical Assessment of C, N and P Fluxes

Hannah L. Bourne[1], James K.B. Bishop[1,2], Todd J. Wood[2], Timothy J. Loew[2] and Yizhuang Liu[1]

[1]Department of Earth and Planetary Sciences, University of California, Berkeley, Berkeley, 94720, USA
[2]Lawrence Berkeley National Laboratory, Berkeley, 94720, USA

Correspondence to: H. L. Bourne (hbourne@berkeley.edu)

Abstract. The magnitude and controls of particulate carbon exported from surface waters and its remineralization at depth are poorly known. The Carbon Flux Explorer (CFE), a Lagrangian float-deployed imaging sediment trap, has been designed to optically measure the hourly variations of particle flux to kilometer depths for months to seasons while relaying data in near-real time to shore via satellite without attending ships. The main optical proxy of particle load recorded by the CFE, volume-attenuance (VA; units of mATN-cm^2), while rigorously defined and highly precise, has not been robustly calibrated in terms of particulate organic carbon (POC), nitrogen (PN), and phosphorus (PP). In this study, a novel 3D printed particle sampler using cutting edge additive manufacturing was developed and integrated with the CFE. Two such modified floats (CFE-Cals) were deployed a total of 15 times for 18-24-hour periods to gain calibration imagery and samples at depths near 150 meters in four contrasting productivity environments during the June 2017 California Current Ecosystem – Long Term Ecological Research (LTER) process study. Regression slopes for VA: POC and VA:PN (units mATN-cm^2: mmol; R^2 in parentheses) were 10.07×10^3 (0.86), 10.05×10^4 (0.87) respectively and was not sensitive to environment or classes of particles sampled. PP was not strongly correlated with VA.

1 Introduction

Marine phytoplankton account for about half (or 50 Pg C y^{-1}) of global primary productivity and live for one week on average before being consumed by zooplankton (Falkowski et al., 1998). Approximately10 Pg C y^{-1} is exported from the surface layer as sinking aggregates containing both particulate organic and inorganic carbon (POC and PIC). The carbon that reaches the deep ocean remains isolated from the atmosphere for centuries. This process, the “biological carbon pump” (BCP), is a fundamental player in the global carbon cycle. The stability of the BCP and its future in the face of climate forced circulation changes and ocean acidification are currently unknown. A number of recent studies have noted discrepancies in reconciling meso- and bathypelagic activity with current euphotic zone flux estimates (Banse, 2013; Burd et al., 2010; Ebersbach et al., 2011; Passow, 2012; Stanley et al., 2012). Recent estimates of carbon flux out of the euphotic zone range from 6 to 12 Pg C y^{-1} (Dunne et al., 2005; Siegel et al., 2014; Yao and Schlitzer, 2013). More traditional methods of measuring particle flux in the ocean rely on sediment traps or geochemical sampling that require ship time (Buesseler et al., 2007). As ship time is expensive both in terms of funding and labor, flux measurements conducted this way are temporally and spatially limited. In recent years, there have been a number of developments towards autonomous instruments capable of measuring particle flux (Bishop et al., 2004, 2016; Briggs et al., 2011; Estapa et al., 2013, 2017).

The attenuation of light by particles has long been used by oceanographers as a measurement of particle concentration in the ocean water column, beginning with development of underwater transmissometers in the early 1970s (Zaneveld, 1973). Transmissometer beam attenuation coefficient (at 660 or 650 nm) has been shown to strongly correlate with measurements of particulate organic carbon (POC) concentration in the water column (Bishop et al., 1999; Bishop and Wood, 2008; Boss et al., 2015; Gardner et al., 2000). Transmissometers were first deployed vertically mounted on Lagrangian profiling floats (called the Carbon Explorers, CEs) in 2001 in the North Pacific (Bishop et al., 2002). These deployments revealed a systematic loss of transmission as the CEs drifted at depth between profiles. A trend of increasing transmission was seen in the deepest 200-300 m as the float rose from 1000 m to the surface, implying that particles had accumulated on the upward looking transmissometer window during drift and were being washed off during initial stages of profiling. CE's deployed in the Southern Ocean in 2002 were modified to measure transmittance before and after exhaust flow from the float's CTD pump was used to clean particles off the transmissometer window during drift and thus a Carbon Flux Index (CFI) was derived as a systematic measure of particle flux over time (Bishop et al., 2004). Estapa et al. (2017) advanced the quantitative use of float-deployed transmissometers to estimate particulate carbon flux and more properly derived a flux proxy based on beam attenuance change over the 1-2 days that their neutrally buoyant traps drifted at depth. The Estapa et al. (2017) method does not involve optics flushing.

The Carbon Flux Explorer (CFE), which combines an imaging Optical Sedimentation Recorder (OSR) and profiling Sounding Ocean Lagrangian Observer (SOLO) float, periodically images particles as they accumulate on a glass sample stage. It thus builds upon the concept of optically measuring particle flux by quantifying particle attenuance at each pixel (Bishop et al., 2016; Bishop and Wood, 2009). The imaging instrument also fully resolves particle classes from 20 μm to cm scale. As transmissometer beam attenuation coefficient was found to be highly correlated to POC concentration, a reasonable assertion would be that light attenuance of particles integrated across an image (volume attenuance) would also be highly correlated to POC load. Image attenuance (ATN) is the combined effect of both light scattering loss and light absorption by particles, it is calculated by taking the $-\log_{10}$ of a transmitted light image normalized by an *in-situ* blank composite image of the particle free sample stage (Bishop et al., 2016). Integration of ATN across the sample stage area yields Volume Attenuance (VA, units: mATN-cm^2), a measure of particle load. Normalizing by trap opening and time deployed yields Volume Attenuance Flux (VAF, units: mATN-cm^2 cm^{-2} d^{-1}).

Successful calibration of VAF in carbon units would allow for far greater temporal, and spatial resolution of carbon export than possible with ships and thus inform current models of biological carbon flux as CFEs have the capability of observing hourly variation of particle flux at depth for months to seasons (Bishop et al., 2016). An earlier attempt to calibrate the CFE in 2013 used a surface tethered OSR and sampler (shown in Mcdonnell et al., 2015 Fig. 3F). This method failed as it was discovered that simultaneously deployed surface-tethered OSRs and Lagrangian CFEs collected far different particle types, size distributions, and quantities of material (Bishop et al., 2016). The surface-tethered OSR was biased low by as much as a factor of 20 and collected almost no material larger than 1.5 mm. These larger aggregates encounter the cm sized openings of the trap in a near horizontal trajectory and thus bounce back into the flow rather than accumulating in the trap. Lacking calibration samples, Bishop et al. (2016) utilized aggregate size – POC weight estimates from Bishop et al. (1978) to derive a factor of 2.8 for scaling VAF (mATN-cm^2 cm^{-2} d^{-1}) to POC flux (mmol C m^{-2} d^{-1}); they note that applying the Alldredge (1998) volume-POC formula for marine snow particles collected by scuba in shallow waters yielded a conversion factor of 0.16, about 17 times smaller than the estimate based on Bishop et al. (1978).

Estapa et al. (2017) working in oligotrophic waters near Bermuda compared sediment trap POC flux with transmissometer attenuance drift (at 650 nm); conversion of their results (Fig. 7 in Estapa et al., 2017) yielded factors ranging from 0.46 to 0.74 (in our units of VAF: POC), four to six times lower than our 2.8 conversion factor (a conversion error in Estapa et al., 2017 implied a greater difference). Multiple optical reasons for differences include: (1) beam collimation (CFE uses a diffuse LED light source and camera (Bishop et al. 2016) whereas transmissometers are highly collimated but can vary a factor of two in sensitivity based on differences of beam geometry and receiver acceptance angle (Bishop and Wood, 2008; Estapa et al., 2017), (2) effects of particle size distribution on attenuance, (3) wavelength dependence of attenuance (CFE uses the green image plane (~550 nm) vs. red transmissometer (650 nm)), and (4) stray light. Estapa assumed 100% collection efficiency of particles on the vertically facing transmissometer window and zero contribution of optics biofouling to her measurements. The difference in slopes may be also method dependent as Estapa et al. (2017) analyzed only the particulate carbon in 350 µm screened material from the neutrally buoyant sediment traps whereas the Bishop et al. (2016) factor is based on larger aggregates up to cm size.

Given our finding of a factor of 20 under collection of sample by the surface-tethered OSR, a great uncertainty of literature-based calibration factors, the few environments sampled, and the multitude of lighting and methodological factors affecting the relationship of attenuance and carbon, we needed to develop a particle sampling device which could operate on the CFE. The new integrated system is referred to as "CFE-Cal" (Fig. 1a).

Below we describe important design advances that led to the CFE-Cal and report first results from 2 CFE-Cals that were deployed and recovered 15 times at four locations during the June 2 to July 1 2018 California Current Ecosystem Long Term Ecological Research (CCE-LTER) process study cruise aboard R/V *Revelle*. The aim of the CCE-LTER expedition was to characterize food web processes and particle export at different places within and outside of an offshore-flowing phytoplankton-rich filament of upwelled water near Point Conception, CA (Fig. 1b). The diverse environments sampled provided an excellent opportunity to collect a calibration sample dataset under high to low particle flux conditions.

2 Materials and Methods

2.1 CFE, CFE-Cal and Optical Attenuance

Bishop et al. (2016) describe in detail the CFE and the operation of its particle flux sensing OSR. These core elements are identical to those of the CFE-Cal. Briefly, once released from the ship the CFE dives repeatedly below the surface to obtain OSR observations at up to three target depths as it drifts with currents. The CFE's OSR awakes when the target depth is reached. Particles settle through a hexagonal celled baffle (1 cm opening) into a high-aspect ratio funnel assembly before depositing on a 2.54 cm diameter glass sample stage. Particles are imaged at 13 µm pixel resolution in three lighting modes: transmitted, transmitted–cross polarized, and dark field. In this paper, we focus only on the calibration of POC sample loading vs. volume attenuance determined from transmitted light imagery.

On first wake-up of a given CFE dive, the sample stage is flushed with water and images of the particle-free stage are obtained. At timed intervals (~25 min in data described here) the OSR repeats image sets, which register the sequential buildup of particles. After the predetermined number of image sets over ~1.8 h, cleaning occurs and a new reference image set is obtained. After ~5-6 h at a target depth, the OSR performs a final image set, cleaning cycle and reference image set, and the CFE surfaces to report GPS position, CTD profile data and OSR engineering data, and dives to its next target depth. All target depths in this study were chosen to be at 150m. We describe in detail below the particle sampler and its integration with the CFE to form the CFE-Cal. In the case of the CFE-Cal, stage cleaning operations direct particles from each dive to a unique sample bottle.

Image attenuance was calculated following Bishop et al. (2016). Briefly, transmitted light images were normalized by a composite in-situ image of the particle free sample stage. The $-\log_{10}$ of the normalized image was taken to yield ATN values. Pixels with a light attenuance value less than 0.02 were defined to be background. Pixels with attenuance values above 0.02, determined to be particles, were integrated across the sample stage then divided by total number of pixels in the sample stage area yield attenuance. This is multiplied by 1000 to yield mATN and then by the sample stage area to give sample Volume Attenuance (VA, units: mATN-cm^2).

Depth seeking performance of the CFE-Cal, imaging and sampling times, and derived VA time series are illustrated in Figure A1. In order to compare VA to filter loads of POC, PN and PP, the cumulative VA over the course of a dive had to be calculated. During a dive, particles are transferred from image stage to a specific sample bottle between 2 to 6 times. For each cleaning cycle, the VA of a clean image was subtracted from the image with particles prior to transfer to a bottle. This then represented the amount of material directed into the sample bottle after cleaning. VA from each cleaning step was then summed to yield a cumulative VA which should correspond exactly to the particles directed into the sample bottle (Table S1).

2.2 Sampler

Most key components of the sampler for the CFE-Cal were fabricated in the Advanced Prototyping Lab at the Jacobs Institute for Design Innovation at UC Berkeley using a Multi-Material Color Objet260 Connex3 (Stratasys, Israel); some parts were also fabricated using the Carbon model M1 3D printer (Redwood City, CA). We chose these particular additive manufacturing processes because they were fast, low-cost, and enabled improved functional designs that were impossible to machine.

The new sampler incorporates the operation and water flow logic of a sampler built in 2004 for our surface buoy-tethered OSR (Fig. 7F in McDonnell et al. 2015; Bishop et al., 2016). The physical layout of the sampler is entirely new as the CFE-Cal had to meet stringent dimensional, buoyancy, compressibility, drag performance, and tilt criteria. Furthermore, as the sampler is intended to collect samples for particulate carbon, nitrogen, phosphorous, calcium carbonate, silica, and trace metals, it needed to be non-contaminating.

Figure 2a shows detail of the integration of the sampler with 4 mounted sample collection bottles on the CFE-Cal; Figs. 2b and 2c detail the particle isolation system within each sample bottle. A gear motor (2842S024C; Faulhaber Group, Micromo, Florida) and related custom electronics which actuate the sampler are housed in a pressure compensated acrylic tube filled with Fluorinert (3M) fluid and is mated coaxially with the rotor (Fig. 2d). Figure A2 shows details of the design of key 3D printed elements of the sampler. The sampler inlet is connected to the particle settling stage by a 40 cm long 9.5 mm inner diameter (ID) polyethylene tube (seen in Fig. 2a) and its outlet is connected by a second 20 cm polyethylene tube to a SBE Model 5T (2000 RPM) pump (Sea Bird Electroncs, WA). Flow rate during cleaning was ~ 20 mL s^{-1}. When the CFE reaches depth on a new dive, the rotor is moved to select a water path that bypasses the sample bottles (Fig. A2, port 0) and the flow is directed to the outlet manifold. The bypass cleaning volume is ~800 mL. After a cycle of particle accumulation and imaging, the motor driven sampler rotator opens to one of four sample bottle positions (1 – 4, Fig. A2) and the suction action of the pump draws water and particles from the imaging stage into the selected 250 mL conical clarified polypropylene centrifuge tube (Thermo Scientific, Nunc). A total of ~400 mL of water is drawn through the sampling system during each regular cleaning cycle and represents about a 30% of the volume of the collection funnel (~1460 cm^3). All particle transfers from a dive are directed to the same bottle (diamond points in Fig. A1). Particles are retained in the bottle by a 14 cm diameter circle of 51 µm polyester 33% open area mesh (SEFAR 07-51/33) wrapped and secured using silicone o-rings around the outlet structure within the bottle (Fig. 2c). The area of perforated outflow cylinder was ~30 cm^2; however, when the circular mesh was secured to the top of the outlet cylinder by an o-ring, the pleated mesh area exposed to flow was ~130 cm^2 (Fig. 2c).

The flow from imaging stage to bottle is constricted by the six 3 mm diameter openings that surround the sample stage. Loosely aggregated material is likely broken up into smaller pieces while being transferred. For cohesive aggregates and rigid particles (such as some Pteropod shells), the upper size limit is 3 mm.

2.3 Sampler Materials

Little is known about water absorption properties, dimensional stability, and chemical reactivity and contamination potential of the 3D printing resins as most are proprietary. The majority of sampler parts were fabricated using the Connex3 from FullCure 720 resin (Fig. A2) and some of the particle isolation assemblies were printed in both FullCure 720 and VeroWhite RGD35 resins. The Connex3 is a fused deposition modeling (FDM) printer which builds parts layer by layer. We fabricated three additional particle isolation assemblies from amber Cyanate Ester, black rigid Polyurethane and black Polylactic (PLA) resins on the Carbon printer; the process uses photopolymerization to form a solid piece as material is drawn from liquid resin. After parts were printed and support material removed, the parts were rinsed with deionized water and then leached in a 1.2 M HCl solution for 16 hours at room temperature. All remained stable to this treatment. Dimensional tests before and after sea trials showed that dimensions of the sampler body (Fig. A2) printed with FullCure 720 remained stable to within 0.06% of design dimensions.

2.4 Field Procedures

Prior to each deployment, the CFE's sample stage and related glass surfaces were cleaned to remove any remaining material collected during the previous deployment. Areas between glass layers were flooded with water to prevent air bubbles being trapped. Each CFE-Cal was outfitted with four clean sample collection tubes and filled with 0.4 µm filtered seawater. On recovery of the CFE-Cals, the sample bottles (Fig. 2d) were either immediately removed from the sampler and filtered or placed in a fridge at 10 °C to minimize sample degradation; in the latter case, samples were processed within 3 hours of collection.

All sample processing and manipulation took place in a laminar flow bench at sea. Each sample was decanted into an open filter funnel loaded with either 47 mm diameter Whatman Quartz Fiber (QMA, pore size ~1.2 µm) or Supor (pore size 0.4 µm) filters; transfer took place with filters under mild suction with the aim of evenly covering the filter surface (Fig. A3). Each sample tube and associated 51 µm mesh were further rinsed three times with ~ 5 mL of 0.4 µm filtered seawater to ensure quantitative transfer of particles. After filtration, the samples were quickly misted with ~3 mL of deionized water (DI) to reduce residual sea salt while still under suction. Samples were then placed in Gelman Petri slides and photographed wet under

LED ring light illumination using a 20 Mpixel Sony RX100 V camera (pixel resolution of 19 µm), dried at 50 °C for 24 hours, and photographed again under the same lighting conditions in a laminar clean air bench. Dried samples were then stored in covered peri slides until analyzed in the laboratory. Prior to use, the QMA filters were placed in a muffle furnace at 450 °C overnight to reduce carbon blanks. Both the QMA (after combustion) and the Supor filters were leached in a 1.2 M HCl solution for 24 hours at room temperature and rinsed with deionized water and air dried in a class 100 laminar flow bench prior to use.

2.5 Laboratory Procedures

2.5.1 Carbon and Nitrogen Analysis

Briefly, half of each QMA filter was placed in a desiccator and exposed to HCl fumes (from 12 M HCL) for 24 hours to remove any carbonate carbon (Bishop et al. 1978) and then dried at 30°C for 36 hours and subsampled 6 to 8 times using a 3 mm diameter biopsy punch yielding ~1/16th of the whole sample. These were loaded into tin capsules and analyzed for total organic carbon and nitrogen using a Thermo Quest EA2500 Elemental Analyzer at Oregon State University according to Holser et al. (2011). A total of 27 unique cruise samples and process blanks (with 6 replicates), 5 unused QMA filters, and analytical blanks (empty tin capsules) were run. Process blanks were samples where no particles were directed to sample tube during deployment and processesed as other samples. The other half of the sample was preserved for ICP-MS analysis.

Samples ranged from 0.0267 to 0.1570 mmol C/filter (average ± sd: 0.0760 ± 0.0362) and 0.0029 to 0.0155 mmol N/filter (average ± sd: 0.0065 ± 0.0034). Process blanks contained 0.032 ± 0.008 mmol C/filter and 0.003 ± 0.0003 mmol N/filter. Unused QMA blanks were 0.0037 ± 0.0008 mmol C/filter and were below the detection limit for nitrogen; only 12% of carbon in the process blanks came from the blank filter. Nearly 90% of the process blank carbon is due either to accidental collection of particles during deployment, contamination during initial processing, or from DOC adsorption. Particles may enter a sample bottle while the sampler is turning and the selector briefly passes the blank bottle inlet. Data are tabulated in Table S1.

Replicate analysis of 4 samples gave an average RSD of 0.14 and 0.07 for C and N, respectively which we assume is attributed to sample heterogeneity and can be applied to all samples. The RSD for replicate analyses of process blanks was 0.18 and 0.12 for C and N.

Corrected POC was calculated following Eq (1):

$$POC_{corrected} = POC_{measured} - POC_{process\ blank}$$

The sample POC error was calculated following Eq (2):

$$POC_{error} = \sqrt{(process\ blank\ s.d.)^2 + (sample\ RSD \times POC_{corrected})^2}$$

Nitrogen and phosphorous were calculated the same way, replacing POC with PN and PP.

2.5.2 ICP-MS Phosphorous Analysis

Samples on both Supor and QMA filters were analyzed using a Thermo Fisher Element II XR Inductively Coupled Plasma Mass Specrometer (ICP-MS) at the UC Santa Cruz Marine Analytical Laboratory following Bishop et al. (2012). Half of each 47 mm filter was leached in 10 mL of a 0.6 M HCl solution at 60°C for 16 hours. The leach solution was then diluted with 18.2 mOhm-cm Milli-Q DI water to 50 grams; 1 mL of the diluted solution was then further diluted with 3 mL of 0.12 M HCl and spiked with 0.2 mL of 25 ppb In. Standards were prepared in the same acid matrix. Phosphorous in samples ranged 40-fold from 3.9×10^{-5} to 1.5×10^{-3} (average ± sd: $2.0\times10^{-4} \pm 2.4\times10^{-4}$). Unlike C and N, the process blanks were location specific with averages of $8.9\text{x}10^{-5}$, 5.0×10^{-5} , 1.9×10^{-5} and 5.0×10^{-5} mmol P/filter for location 1, 2, 3 and 4 respectively.

3 Results and Discussion

3.1 Samples Collected

Samples were collected from four productivity regimes and environmental conditions yielding a diverse array of particle sizes and classes (Fig. 3a-e). The flux rates between locations also varied widely. At location 1, flux was at times dominated by 1 mm diameter, 5-10 mm long anchovy pellets similar to those described by Saba and Steinberg (2012) with 95% of VA flux (average ~40 mATN-cm^2 cm^{-2} d^{-1}) being carried by particles > 1.5 mm in size. In contrast, at location 2, numerous small diameter (200-300 µm) olive green ovoid pellets dominated imagery and accounted for ~ 50% of the ~15 mATN-cm^2 cm^{-2} d^{-1} VA flux. Location 3, in transitional waters near the filament edge, had a VA flux of ~2.3 mATN-cm^2 cm^{-2} d^{-1} and ~65% of the flux carried by aggregates larger than 1.5 mm. At Location 4, in the most extended part of the filament, VA flux was ~ 22 mATN-cm^2 cm^{-2} d^{-1}, and 94% of the flux was carried by aggregates >1.5 mm in diameter.

The CFE-CALs were deployed 15 times over the course of the June 2017 CCE-LTER study, CFE-Cal malfunction (i.e. instrument not diving to depth, not stabilizing at depth, or sampler not switching target bottles correctly) or swimmers such as a large siphonophore (see Table 1 for details) led to some dives not yielding usable samples. Altogether, there were 19 valid QMA samples (15 samples, 4 blanks) and 27 Supor samples (19 samples, 8 blanks).

3.2 Collection Efficiency

To validate the efficiency of transfer of particles imaged to sample bottles, ovoid pellets were manually counted (Fig. 4) in both the CFE's OSR images and of photographs of filters of material sampled at location 2. CFE002 collected close to the same number of particles in the sampler as were imaged. CFE004 collected 1.45 times more ovoid pellets in the sampler than were imaged. We don't fully understand this but known sampler positioning issues at this time may have led to transfer of pellets to bottles from times (such as during float ascent to the surface) when particles were not imaged by CFE004. To correct for this, the POC, PN and PP numbers for CFE004 at location 1, 2 and 3were divided by 1.45. A software problem was identified and addressed prior to location 4 deployments and no correction was applied.

Bishop et al., (2012) investigated the effect of filtration rate on aggregate retention during large volume in-situ filtration sampling and found that aggregates were broken up when the flow velocity through 51 µm mesh exceeded 1 cm s^{-1} over a four-hour sampling time. During CFE-Cal stage cleaning, the sample transfer pump is operated for two cycles of ten seconds at a flow rate of ~20 mL s^{-1}. The mesh area on the outflow from the sample bottle is approximately 130 cm^2. We thus calculate the flow speed through the mesh to be ~0.15 cm sec^{-1}, 15% of the threshold speed recommendation by Bishop et al. (2012). Although intact large aggregates were not seen on the sample filters (compare Fig. A3d vs. Fig. 3d), given our limited sample collection time (< 2 minutes) and low flow velocity, we believe that our transfer efficiency for the particles comprising the loosely aggregated material is similar to that for the more robust pellets.

3.3 Calibration Results

Figure 5 shows cumulative VA regressed against sample POC, PN and PP (data in Table S1). All of our results are forced through zero as both VA and elemental values are blank controlled. Regressions results yielded slopes and R^2 values (in parentheses) of 10,066 mATN-cm^2: mmol POC (0.86) and 100,500 mATN-cm^2: mmol PN (0.87). Three of 16 samples had C/N ratios above 20 and were not used in the regression for POC as these numbers are not typical of sinking particles (e.g. Bishop et al., 1977, Lamborg et al., 2008, Stukel et al., 2013). Stukel et al. (2013) reported trap POC/PN mole ratios ranging from 5-14 (average, 9.6) at 100 m in the same upwelling regime we have sampled; Lamborg et al. reported POC/PN ratios ranging from 7.7 to 8.5 in productive waters of the Oyashio and Oligotrophic waters of the North Pacific Gyre. The molar ratio of C/N from our regression slopes is 9.92, in line with Stukel et al., 2013. The data also demonstrate that there is no obvious difference for VA:PN or VA: POC for samples collected from Locations 1 and 4 (Fig. 1, Fig. 4) where aggregates > 1.5 mm in size accounted for 95% of the flux compared to Locations 2 and 3 where smaller material contributed 50 and 30% of the flux, respectively.

The high C/N values of excluded samples may have been due to contamination by residual material used as a scaffold to build the 3D printed parts; in one case, a 1 mm sized aggregate of such material was found on our filters. The scaffold material, Stratasys' OBJET Support SUP706 is made of 1,2-Propylene glycol and Polyethylene glycol, Methanone, (1-hydroxycyclohexyl) phenyl-both of which contain carbon but not nitrogen (SUP706 SDS https://store.stratasys.com/medias). The material also contains an unspecified acrylic. The regression of cumulative VA: POC is less significant than VA:PN. Part of this is due to the greater relative variability of carbon blanks versus nitrogen blanks. We further believe that some carbon may have originated as transparent exopolymer particles (TEP), produced by phytoplankton and bacteria, whereas nitrogen is not a component of TEP (Alldredge et al., 1993). TEP is seen only through staining and electron microscopy and is invisible to standard light imaging. The ratio of VA:POC of a sample would be altered due to the presence of TEP as POC concentrations would increase, but VA would not change. The ratio of VA:PN however remains stable whether or not TEP is present.

The relationship for VA: PP was scattered with a slope of 1,543,000 mATN-cm^2: mmol PP (-0.07, negative r^2 values denote results worse than horizontal fit). One sample heavily laden with anchovy fecal pellets had a PP content far higher than all other samples (POC/PP ratio ~90) and when this point was removed the relationship of VA: PP improved 3,23,000 mATN-cm^2 : mmol PP (0.41). The fact that PP had the lowest correlation with VA is consistent with the strong loss of P relative to carbon and nitrogen as large aggregates sink (e.g. Bishop, 1977; Lam et al., 2007). Scanning electron microscopy showed that the anchovy fecal pellets were stuffed with diatoms and as they are larger and sink at a much faster rate (up to 500m in one day), it follows that this sample should have a higher PP content as there is less time for microbial degradation and remineralization.

The ratio of C/P using the regression slopes is 152 with slope including high P sample, and 321 excluding it. These C/P ratios both agree well with pooled results for >53 µm particles sampled from depth interval 100-200 m in the Eastern Equatorial Pacific (Bishop, Stepien and Wiebe, 1986), Atlantic (Bishop et al., 1977), and waters of the Southern Ocean (Lam and Bishop, 2007) which had an average Corg/P = 211 (range 137 to 360). They also fall in the range Lamborg et al. (2008) reported for 150 m trapped material at the VERTIGO Aloha (range 238 – 409) and Oyashio regimes (83-180).

3.4 Comparison to previous studies

Two autonomous flux monitoring systems, the CFE (Bishop et al., 2016) and the OST (Estapa et al., 2017), have now been calibrated to relate the attenuance flux to the flux of particulate organic carbon. This study expands upon Estapa et al. (2017) as samples from a wider range of environments have been collected and a far greater range of aggregate size distributions were observed. The highest POC flux collected in Estapa et al.'s (2017) calibration was under 2 mmol C m^{-2} d^{-1}. The flux environments sampled in our study ranged from <2 to 40 mmol C m^{-2} d^{-1}.

Figure 6 compares the relationship between VA flux and carbon flux from this study vs. data from Estapa et al. (2017) (data for regression in Table S1). When converted to compatible units, the slope for Estapa's VA flux (mATN-cm^2 cm^{-2} d^{-1}) versus POC flux (mmol C m^{-2} d^{-1}) is 2.19 (forced through zero) and 1.50 (allowing for an intercept) while our slope is 1.03 (forced through zero). Our observations were for depths near 150 meters and it is unknown if there is a depth dependence to calibration factors. We note that Estapa et al. (2017) combined samples from ~150, 300 and 500 meters in her regression. This said, the slopes of our two datasets differ by only a factor of 2. In our data, attenuance of particles in the red image plane is 6% lower than in green, thus wavelength of analysis is a minor factor explaining the differences. Given the large range in particle size distributions, we can rule out particle size effects. Beam geometry and the other factors underlying our different methodologies likely explain the differences found.

Bishop et al. (2016) estimated the factor for conversion of POC flux (C mmol m^{-2} d^{-1}) to VA flux (mATN-cm^2 cm^{-2} d^{-1}) to be 2.8; the reverse conversion factor is 0.357 consistent with slopes depicted in figure 6. Analysis of directly imaged and sampled material in this study yielded a slope of 1.03, which is about 3 times higher than estimated using Bishop et al., (1978) but 6 times lower than inferred from Alldredge's (1998) relationship for marine snow sampled by scuba from shallow depths. Our results are not consistent with the published Alldredge (1998) relationship.

Bishop et al. (2016) reported CFE attenuance fluxes averaging 66.2 mATN-cm^2 cm^{-2} d^{-1} at 150 m in the Santa Cruz Basin in January 2013 and estimated a POC flux of 190 mmol C m^{-2} d^{-1}, about 8 times higher than the highest previously measured flux from surface-tethered sediment traps deployed over a 3-year period at 100 and 200 meters in nearby waters (Thunell, 1998; August 1993 to September 1996). Converting the 66.2 mATN-cm^2 cm^{-2} d^{-1} attenuance flux to POC flux using our new calibration yields 68.19 mmol C m^{-2} d^{-1}, a value which is still three times higher than the highest previously measured flux (Thunell, 1998). In short, the likely discrimination of surface tethered baffled sediment traps against the collection of >1 mm sized particles remains an issue in biologically dynamic regimes dominated by large aggregates.

4 Conclusions

The development of a sampling system for the Carbon Flux Explorer has overcome a major barrier to the calibration of our attenuance proxy for organic matter export. The calibration of volume attenuance flux (VAF) against organic carbon, nitrogen and phosphorus flux in this study represents an important step forward in the development of autonomous optical flux measurements. Our regression results yield strong calibrations for POC and PN (POC $R^2 = 0.86$ and PN $R^2 = 0.87$) that apply over a wide range of environments. If TEP does contribute to POC flux in our samples, then our results suggest that attenuance is a better proxy for particulate nitrogen flux. Phosphorus was shown to be poorly correlated, consistent with the highly labile nature of this element relative to either C or N. Our results give us confidence that images collected by the CFE can be used to calculate the fluxes of carbon and nitrogen. In addition, our calibration is shown to be insensitive to particle size distribution and particle classes dominating export. We find less than a two-fold difference in the POC flux vs. Volume Attenuance flux regression slope from Estapa et al. (2017). This is remarkable given the strongly different environments, methodology, and means by which fluxes were sampled. Both these studies reinforce the theory that light attenuation can be used as a proxy for POC and in our case PN flux. As all calibration samples in this dataset were made at 150 m, in the future we plan calibration studies to include more depths to 1000 meters. Intercalibration of the CFE attenuance measurements with other autonomous systems should be pursued. Results presented above demonstrate that the magnitude of flux and of food web processes responsible for flux can vary strongly over relatively small spatial and temporal scales in dynamic coastal waters. Thus, the use of high frequency autonomous observations will significantly better inform food web and carbon export simulations. Our successful calibration of VAF in terms of POC and PN justifies expanded deployments of instruments such as the Carbon Flux Explorer in remote and stormy seas.

Acknowledgements

We would like to thank Mark Ohman (chief scientist), members of the science party, and captain and crew of the R/V Revelle for facilitating CFE-Cal deployments during the June 2 – July 1 2017 California Current Ecosystem Long Term Ecological Research process study. Lee-Huang Chen (UC Berkeley, Engineering) contributed at critical stages of this project. We thank Alejandro Morales (LBNL), Christopher Parsell and the Jacobs Institute for Design Innovation at UC Berkeley (UC Berkeley), Christopher Myers (UC Berkeley), Mike McLune (SIO), Phoebe Lam and Rob Franks (UC Santa Cruz). We'd also like to thank the many UC Berkeley undergraduates who have worked with us at sea and in the laboratory, in particular, Casey Fritz, Beth Connors, Xiao Fu, Sylvia Targ, Jessica Kendall-Bar, and William Kumler. US National Science Foundation grant OCE 0936143 supported Carbon Flux Explorer development; OCE 1528696 supported the development and at sea work with the CFE-Cal systems. The CCE-LTER is supported by US NSF grant OCE 16-37632.

References

Alldredge, A.L., Passow, U. and Logan, B.E.: The abundance and significance of a class of large, transparent organic particles in the ocean, Deep Sea Res. Part I Oceanogr. Res. Pap., 40(6), 1131-1140, doi:10.1016/0967-0637(93)90129-Q, 1993.

Alldredge, A.: The carbon, nitrogen and mass content of marine snow as a function of aggregate size, Deep Sea Res. Part I Oceanogr. Res. Pap., 45(4-5), 529-541, doi:10.1016/S0967-0637(97)00048-4, 1998.

Banse, K.: Reflections About Chance in My Career, and on the Top-Down Regulated World, Ann. Rev. Mar. Sci., 5(1), 1–19, doi:10.1146/annurev-marine-121211-172359, 2013.

Bishop, J.K.B., Edmond, J.M., Ketten, D.R., Bacon, M.P. and Silker, W.B.: The chemistry biology and vertical flux of particulate matter from the upper 400m of the equatorial Atlantic Ocean, Deep Sea Res., 24, 511-548, 1977.

Bishop, J.K. B., Stepien, J.C. and Wiebe, P.H.: Particulate matter distributions, chemistry and flux in the panama basin: response to environmental forcing, Progress in Ocean., 17(1-2), 1-59, doi:10.1016/0079-6611(86)90024-8, 1986.

Bishop J.K.B, J., E. Calvert S., S. and Soon, M. Y. S.: Spatial and temporal variability of POC in the northeast subarctic Pacific, Deep. Res. Part II Top. Stud. Oceanogr., 46(11–12), 2699–2733, doi:10.1016/S0967-0645(99)00081-8, 1999.

Bishop, J. K. B. and Wood, T. J.: Particulate matter chemistry and dynamics in the twilight zone at VERTIGO ALOHA and K2 sites, Deep. Res. Part I Oceanogr. Res. Pap., 55(12), 1684–1706, doi:10.1016/j.dsr.2008.07.012, 2008.

Bishop, J. K. B. and Wood, T. J.: Year-round observations of carbon biomass and flux variability in the Southern Ocean, Global Biogeochem. Cycles, 23(2), 1–12, doi:10.1029/2008GB003206, 2009.

Bishop, J. K. B., Ketten, D. R. and Edmond, J. M.: The chemistry, biology and vertical flux of particulate matter from the upper 400 m of the Cape Basin in the southeast Atlantic Ocean, Deep. Res., 25(12), doi:10.1016/0146-6291(78)90010-3, 1978.

Bishop, J. K. B., Davis, R. E. and Sherman, J. T.: Robotic observations of dust storm enhancement of carbon biomass in the North Pacific., Science, 298(5594), 817–821, doi:10.1126/science.1074961, 2002.

Bishop, J. K. B., Wood, T. J., Davis, R. E. and Sherman, J. T.: Robotic observations of enhanced carbon biomass and export at 55 degrees during SOFeX., Science, 304(5669), 417–420, doi:10.1126/science.1087717, 2004.

Bishop, J. K. B., Lam, P. J. and Wood, T. J.: Getting good particles: Accurate sampling of particles by large volume in-situ filtration, Limnol. Oceanogr. Methods, 10, 681–710, doi:10.4319/lom.2012.10.681, 2012.

Bishop, J. K. B., Fong, M. B. and Wood, T. J.: Robotic observations of high wintertime carbon export in California coastal waters, Biogeosciences, 13(10), 3109–3129, doi:10.5194/bg-13-3109-2016, 2016.

Boss, E., Guidi, L., Richardson, M. J., Stemmann, L., Gardner, W., Bishop, J. K. B., Anderson, R. F. and Sherrell, R. M.: Optical techniques for remote and in-situ characterization of particles pertinent to GEOTRACES, Prog. Oceanogr., 133, 43–54, doi:10.1016/j.pocean.2014.09.007, 2015.

Briggs, N., Perry, M. J., Cetinić, I., Lee, C., D'Asaro, E., Gray, A. M. and Rehm, E.: High-resolution observations of aggregate flux during a sub-polar North Atlantic spring bloom, Deep Sea Res. Part I Oceanogr. Res. Pap., 58(10), 1031–1039, doi:https://doi.org/10.1016/j.dsr.2011.07.007, 2011.

Buesseler, K. O., Antia, A. N., Chen, M., Fowler, S. W., Gardner, W. D., Gustafsson, O., Harada, K., Michaels, A. F., Rutgers van der Loeff, M., Sarin, M., Steinberg, D. K. and Trull, T.: An assessment of the use of sediment traps for estimating upper ocean particle fluxes, J. Mar. Res., 65(3), 345–416, doi:10.1357/002224007781567621, 2007.

Burd, A. B., Hansell, D. A., Steinberg, D. K., Anderson, T. R., Arístegui, J., Baltar, F., Beaupré, S. R., Buesseler, K. O., DeHairs, F., Jackson, G. A., Kadko, D. C., Koppelmann, R., Lampitt, R. S., Nagata, T., Reinthaler, T., Robinson, C., Robison, B. H., Tamburini, C. and Tanaka, T.: Assessing the apparent imbalance between geochemical and biochemical indicators of meso- and bathypelagic biological activity: What the @$♯! is wrong with present calculations of carbon budgets?, Deep Sea Res. Part II Top. Stud. Oceanogr., 57(16), 1557–1571, doi:https://doi.org/10.1016/j.dsr2.2010.02.022, 2010.

Ebersbach, F., Trull, T. W., Davies, D. M. and Bray, S. G.: Controls on mesopelagic particle fluxes in the Sub-Antarctic and Polar Frontal Zones in the Southern Ocean south of Australia in summer-Perspectives from free-drifting sediment traps, Deep. Res. Part II Top. Stud. Oceanogr., 58(21–22), 2260–2276, doi:10.1016/j.dsr2.2011.05.025, 2011.

Estapa, M., Durkin, C., Buesseler, K., Johnson, R. and Feen, M.: Carbon flux from bio-optical profiling floats: Calibrating transmissometers for use as optical sediment traps, Deep. Res. Part I Oceanogr. Res. Pap., 120(December 2016), 100–111, doi:10.1016/j.dsr.2016.12.003, 2017.

Estapa, M. L., Buesseler, K., Boss, E. and Gerbi, G.: Autonomous, high-resolution observations of particle flux in the oligotrophic ocean, Biogeosciences, 10(8), 5517–5531, doi:10.5194/bg-10-5517-2013, 2013.

Dunne J.P., Armstrong, R.A., Gnanadesikan, A. and Sarmiento J.L.: Empirical and mechanistic models for the particle export ratio, Global Biogeochem. Cycles, 19(4), doi:10.1029/2004GB002390, 2005.

Falkowski, P. G., Barber, R. T. and Smetacek, V.: Biogeochemical Controls and Feedbacks on Ocean Primary Production, Science, 281(5374), 200-206, doi: 10.1126/science.281.5374.200, 1998.

Gardner, W. D., Richardson, M. J. and Smith Walker O., J.: Seasonal patterns of water column particulate organic carbon and fluxes in the Ross Sea, Antarctica, Deep. Res. Part II Top. Stud. Oceanogr., 47(15–16), 3423–3449 [online] Available from: http://www.sciencedirect.com/science/article/B6VGC-41WBFCW-J/2/24062ec421c6faf7d4e3f12a28f09509, 2000.

Holser, R. R., Goni, M. A. and Hales, B.: Design and application of a semi-automated filtration system to study the distribution of particulate organic carbon in the water column of a coastal upwelling system, Mar. Chem., 123(1–4), 67–77, doi:10.1016/j.marchem.2010.10.001, 2011.

Lam, P.J and Bishop, J.K.B.: High biomass, low export regimes in the Southern Ocean, Deep Sea Res. Part II, 54, 601-638, doi: 10.1016/j.dsr2.2007.01.013, 2007.

C. H. Lamborg, K. O. Buesseler, J. Valdes, C. H. Bertrand, S. Manganini, S. Pike, R. Bidigare, D. Steinberg, S. Wilson, T. Trull.: The flux of bio- and lithogenic material associated with sinking particles in the mesopelagic “twilight zone” of the northwest and North Central Pacific Ocean, Deep Sea Research Part II: Topical Studies in Oceanography, ISSN: 0967-0645, Vol: 55, Issue: 14, Page: 1540-1563. Doi:10.1016/j.dsr2.2008.04.011, 2008

Mcdonnell, A. M. P., Boyd, P. W. and Buesseler, K. O.: Effects of sinking velocities and microbial respiration rates on the attenuation of particulate carbon fluxes, Global Biogeochemical Cycles, 29(2), 175–193, doi:10.1002/2014GB004935, 2015.

Passow, U. and Carlson, C.A.: The biological pump in a high CO_2 world , Mar. Ecol. Prog. Ser., 470, 249–271 , doi: 10.3354/meps00985, 2012.

Saba, G. K. and Steinberg, D. K.: Abundance, composition, and sinking rates of fish fecal pellets in the santa barbara channel, Sci. Rep., 2, 1–6, doi:10.1038/srep00716, 2012.

Siegel, D. A., Buesseler, K. O., Doney, S. C., Sailley, S. F., Behrenfeld, M. J. and Boyd, P. W.: Global Biogeochemical Cycles, Global Biogeochem. Cycles, 28, 181–196, doi:10.1002/2013GB004743, 2014.

Stanley, R. H. R., Doney, S. C., Jenkins, W. J. and Lott, D. E.: Apparent oxygen utilization rates calculated from tritium and helium-3 profiles at the Bermuda Atlantic Time-series Study site, Biogeosciences, 9(6), 1969–1983, doi:10.5194/bg-9-1969-2012, 2012.

Stukel, M.R., M. D. Ohman, C. R. Benitez-Nelson and M. R. Landry: Contributions of mesozooplankton to vertical carbon export in a coastal upwelling system. Mar Ecol Prog Ser. 491, 47–65, doi: 10.3354/meps10453, 2013.

Thunell, R. C.: Particle fluxes in a coastal upwelling zone: sediment trap results from Santa Barbara Basin, California, Deep

Sea Res. Part II Top. Stud. Oceanogr., 45(8), 1863–1884, doi:https://doi.org/10.1016/S0967-0645(98)80020-9, 1998.

Yao, X. and Schlitzer, R.: Assimilating water column and satellite data for marine export production estimation, Geosci. Model Dev., 6(5), 1575–1590, doi:10.5194/gmd-6-1575-2013, 2013.

Zaneveld, J. R. V., Variation of optical sea parameters with depth, in Lecture Series on Optics of the sea, 61, 2.3-1-2.3-22, 1973

Study Loc.	CFE	Latitude (°N)	Longitude (°W)	Dive	Bottle	Filter	UTC Day Start	UTC Day End	Hours	Depth (m)	Depth stdev	Sample Notes
1	2	35.0739	121.1281	40	1	Supor	160.064	160.270	4.944	0.2		CFE-Cal did not dive
1	2			41	2	QMA	160.333	160.500	4.008	70.0	12.3	anchovy fecal pellets
1	2			42	3	Supor	160.623	160.791	4.032	119.4	7.8	anchovy fecal pellets, not analyzed
1	2	34.9978	121.1650	43	4	QMA*	160.849	160.851	0.048	186.0		sampler closed after bottle 4
1	4	35.0885	121.1293	40	1	QMA	160.076					selector failure
1	4			41	2	Supor	160.297					selector failure
1	4			42	3	QMA	160.422					selector failure
1	4	35.0341	121.1862	43	4	Supor	160.732					selector failure
1	2	34.9396	121.2031	50	1	QMA	162.091	162.294	4.872	131.7	10.9	
1	2			51	2	Supor	162.424	162.536	2.688	31.8	4.4	sample not analyzed
1	2				3	QMA*						
1	2	34.8962	121.2032		4	Supor*						
1	4	34.9348	121.1946	50	1	Supor	162.075	162.280	4.908	189.5	7.7	oil under sample stage reticle
1	4			51	2	QMA	162.410	162.412	0.048	286.2		depth unstable, bottle 2 briefly
1	4			52	3	Supor	162.549	162.551	0.048			depth unstable, bottle 3 briefly
1	4	34.8997	121.2165		4	QMA*						
2	2	34.7771	122.0572	60	1	Supor	165.047	165.264	5.208	142.9	3.8	
2	2			61	2	Supor	165.406	165.574	4.032	112.8	4.3	
2	2			62	3	Supor	165.716	165.883	4.008	97.7	4.1	
2	2	34.8651	122.3355		4	QMA	166.024	166.026	0.048			surfaced open at position 4
2	4	34.7742	122.0587	60	1	QMA	165.060	165.278	5.232	160.9	4.2	C:N >20
2	4			61	2	Supor	165.430	165.597	4.008	153.1	5.7	not analyzed, large jelly (not imaged)
2	4			62	3	QMA	165.739	165.900	3.864	150.2	3.0	
2	4	34.8825	122.3499		4	Supor*						
2	2	34.7098	122.3004	70	1	Supor	166.659	166.882	5.352	159.2	5.1	
2	2			71	2	QMA	167.034	167.202	4.032	146.2	5.8	

2	2			72	3	Supor	167.350	167.517	4.008	147.8	3.9	
2	2	34.6771	122.4122		4	QMA*						
2	4	34.7091	122.2998	70	1	QMA	166.673	166.897	5.376	164.2	10.3	
2	4			71	2	Supor	167.044	167.211	4.008	157.6	3.4	
2	4			72	3	QMA	167.364	167.531	4.008	151.5	2.9	C:N >20
2	4	34.6829	122.4185		4	Supor*						
3	2	34.2275	123.1480	80	1	QMA	170.192	170.368	4.224	141.5	6.7	
3	2			81	2	Supor	170.472	170.639	4.008	131.4	3.8	
3	2			82	3	QMA	170.740	170.879	3.336	143.7	6.7	C:N >20
3	2	34.1717	123.0758		4	Supor*						
3	4	34.1129	122.9885	90	1	QMA	171.205	171.414	5.016	173.4	3.3	
3	4			91	2	Supor	171.553	171.721	4.032	160.9	0.1	
3	4			92	3	QMA	171.860	171.903	1.032	148.8	0.8	
3	4	34.0749	122.8673		4	Supor*						
3	2	34.1086	122.9823	90	1	Supor	171.190	171.369	4.296	126.9	4.8	
3	2			91	2	QMA	171.468	171.636	4.032	159.7	5.7	
3	2			92	3	Supor	171.737	171.904	4.008	154.7	3.6	
3	2	34.0714	122.8552		4	QMA*						
4	4	34.4070	123.0958	100	1	Supor	174.180	174.369	4.536	190.6	5.7	
4	4			101	2	Supor	174.489	174.657	4.032	117.3	3.3	
4	4			102	3	Supor	174.767	174.899	3.168	135.0	3.5	
4	4	34.4174	123.0535		4	Supor*						
4	2	34.4032	123.0964	100	1	QMA	174.294	174.354	1.440	165.8	132.5	didn’t settle at depth
4	2			101	2	Supor	174.479	174.646	4.008	139.9	3.0	
4	2			102	3	QMA	174.742	174.903	3.864	129.5		
4	2	34.4216	123.0310		4	Supor*						
4	4	34.4221	123.0133	110	1	QMA	175.187	175.487	7.200	164.0	5.4	
4	4			111	2	Supor	175.599	175.878	6.696	101.7	3.7	
4	4			112	3	QMA	175.989	176.267	6.672	158.6	3.9	

4	4	34.4449	123.0205	113	4	Supor	176.396	176.496	2.400	119.8	1.8	
4	2	34.4218	123.0168	110	1	Supor	175.173	175.469	7.104	162.8	5.5	
4	2			111	2	QMA	175.582	175.859	6.648	159.5	3.4	jelly in sample, was imaged
4	2			112	3	Supor	175.965	176.242	6.648	156.9	3.0	
4	2	34.4335	123.1008	113	4	Supor	176.350	176.516	3.984	153.1	2.3	

* is a blank

Table 1: CFE-Cal 2017 deployments during the California Current Ecosystem Long Term Ecological Research process study

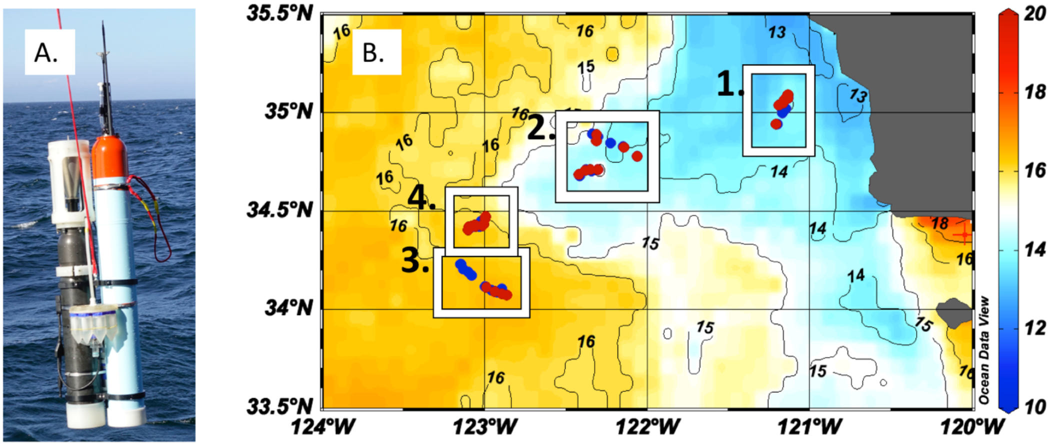

Figure 1: (A) CFE-Cal during deployment from R/V Revelle in 2017. The sampling system for particles is interfaced between the Optical Sedimentation Recorder (left) and SOLO float (right). (B) Map of CFE-Cal deployment and drift locations overlaying map of sea surface temperature (°C) for June 10-17 2017 from NASA Ocean Color Aqua Modis 4km resolution (https://oceancolor.gsfc.nasa.gov/). Blue dots within location boxes represent CFE-Cal 002 and red dots represent CFE-Cal 004 positions.

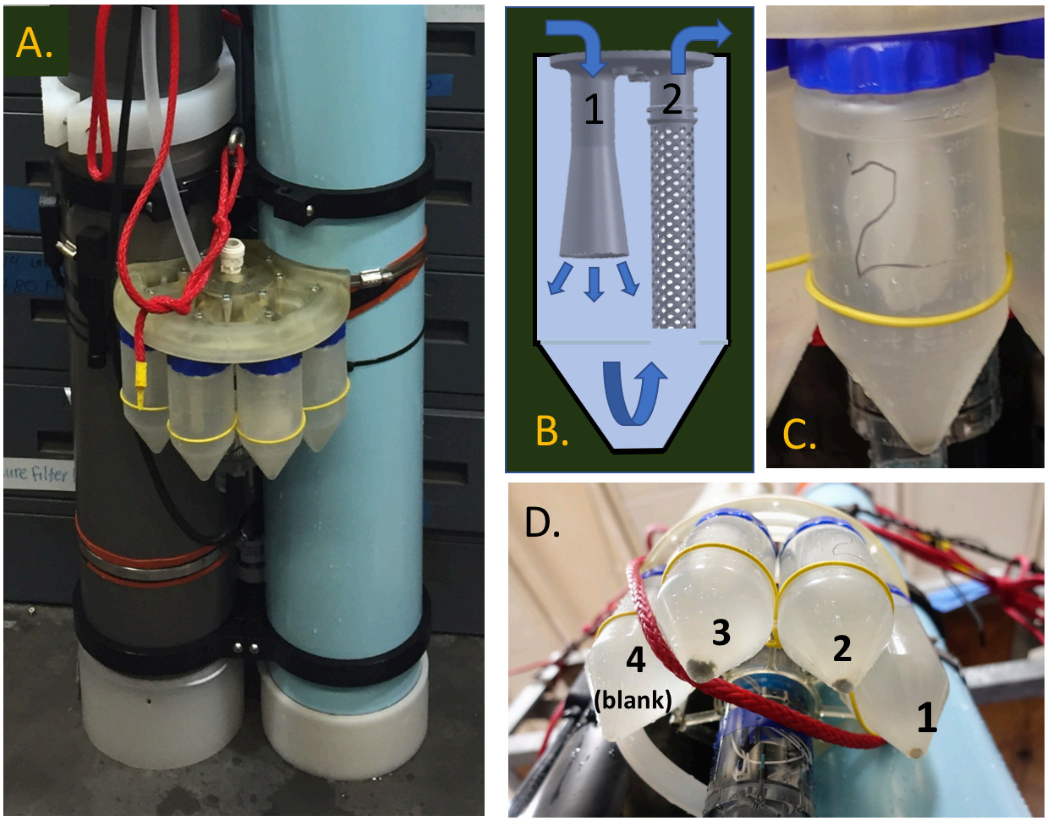

Figure 2: (A) Sampler on CFE-Cal. Suction action of a pump draws water and particles down a poly tube to the sampler (shown disconnected). (B) Detail of particle retention system within sample bottles. Inlet is cone shaped to decelerate incoming flow. Outlet is formed to accommodate 51 µm mesh which is retained by two o-rings at the top. (C) Closeup 5 **of bottle with Mesh filter in place; Filter area is ~130 cm^2. (D) CFE-Cal recovery after 24-hour deployment showing collected samples. Bottle 2 is shown in C. In this case, bottle 4 was a blank (i.e. no particles directed to it).**

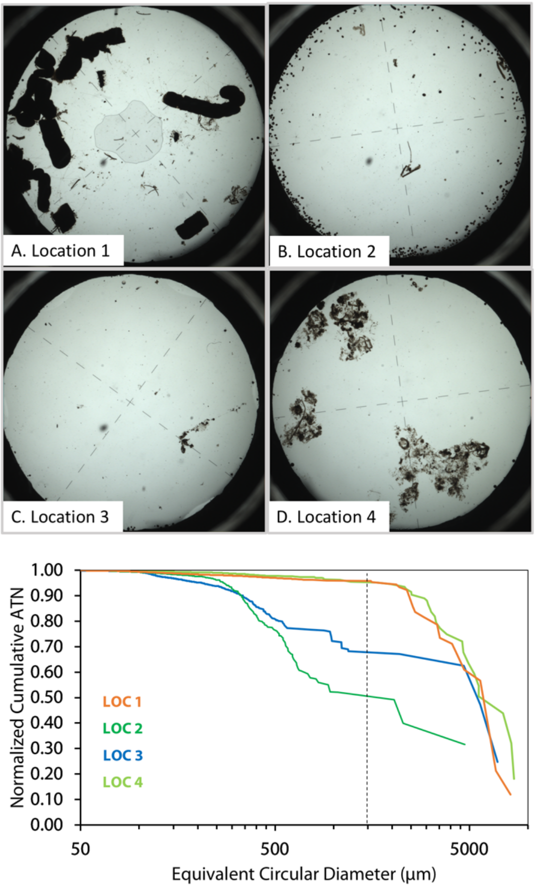

Figure 3: Representative images from four locations. The particle size classes present varied widely at the four different locations. (A) In location 1, flux was dominated by large 1 mm diameter anchovy fecal pellets. (B) Flux was dominated by small ovoid pellets 200-300 microns in diameter. (C) Location 3 was characterized by very low flux. Flux was dominated by small particles with the occasional large aggregate. (D) Flux was dominated by large aggregates. (E) cumulative normalized volume attenuance vs. equivalent circular diameter curves representative of the 4 locations. Approximately 95% of flux was carried by aggregates >1.5 mm in size at locations 1 and 4. Location 2 had ~50% of flux in >1.5 mm fraction.

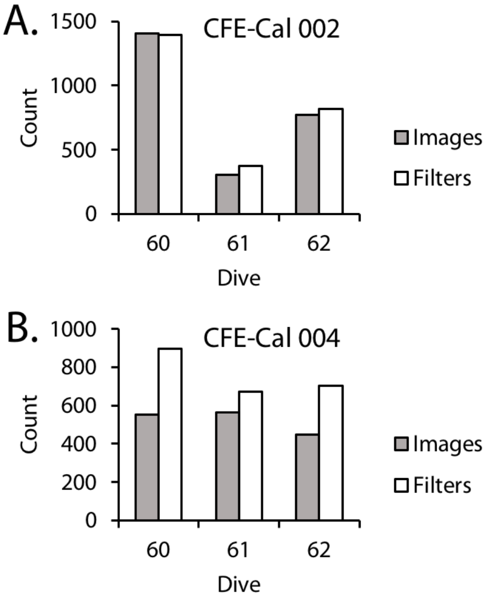

Figure 4: Comparison counts of ovoid pellets in images versus on filters. (A) CFE-CAL002 Deployment 3 (first deployment at location 2) (B) CFE-CAL002 Deployment 4 (second deployment at location 2).

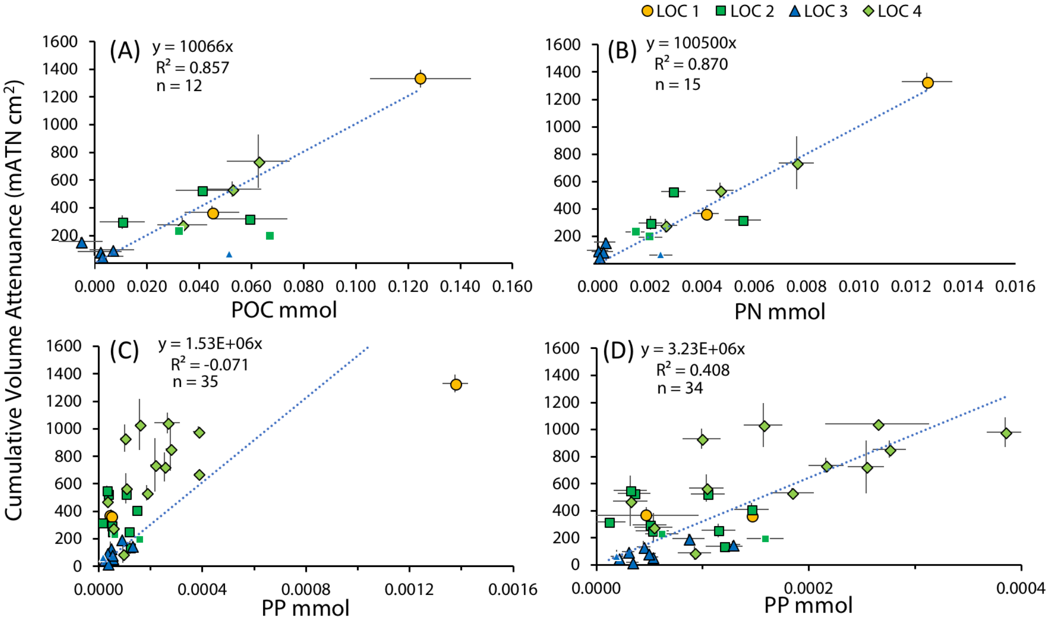

Figure 5: Data and regressions of sample POC (A), PN (B) and PP (C and D) vs. cumulative volume attenuance. Fits are forced through zero. Smaller symbols in all plots denote samples excluded from the POC regression analysis; these had C/N values >20 and were likely contaminated for carbon and not nitrogen. No data was excluded from PN or PP regressions. P regressions (C and D) include and exclude, respectively the high P enriched sample which was dominated by anchovy fecal pellets.

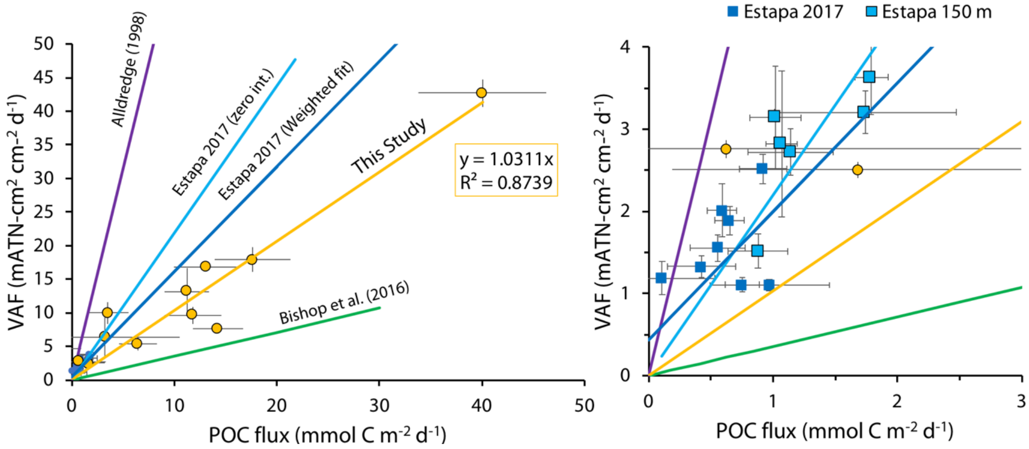

Figure 6: Regressions of ATN-POC (mATN-cm^2 cm^{-2} d^{-1}) to POC (mmol C m^2 d^{-1}) for this study (orange; y = 1.03x , R^2=0.874), Estapa et al. (2017, blue, y = 1.56x + 0.434, R^2 = 0.632; light blue, y = 2.191x, R^2 = 0.47). Bishop et al. 2016 estimated slope (green) is 0.357 (1.0/2.8). Alldredge (1998) estimated slope (purple) = 6.25.

Appendix Figures.

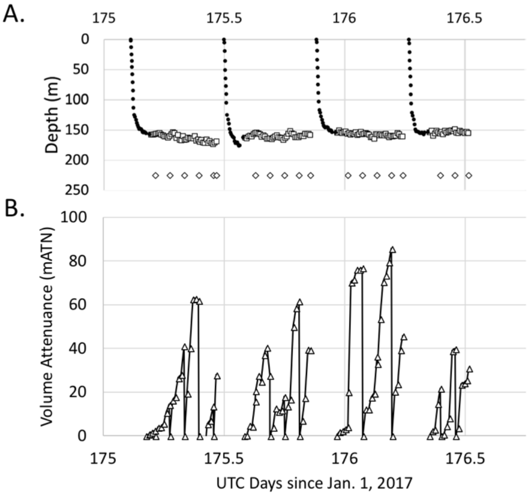

Figure A1: (a) Typical deployment trajectory of a CFE-Cal. The x-axis is time in days (Jan 1 2017 at 1200UTC = day 0.5). The filled black circles are depths as the CFE-Cal is diving, open black squares denote depths as the CFE drifts and takes images of settled particles. The open black diamonds represent times when the sample stage was cleaned and particles directed into a sample bottle. (b) Graph B shows the corresponding attenuance for each photo taken. Particles build-up over time and then periodically the glass stage will be rinsed off and particles directed into the sample bottles. Due to a programming error, the sampler and particles are not removed from the stage.

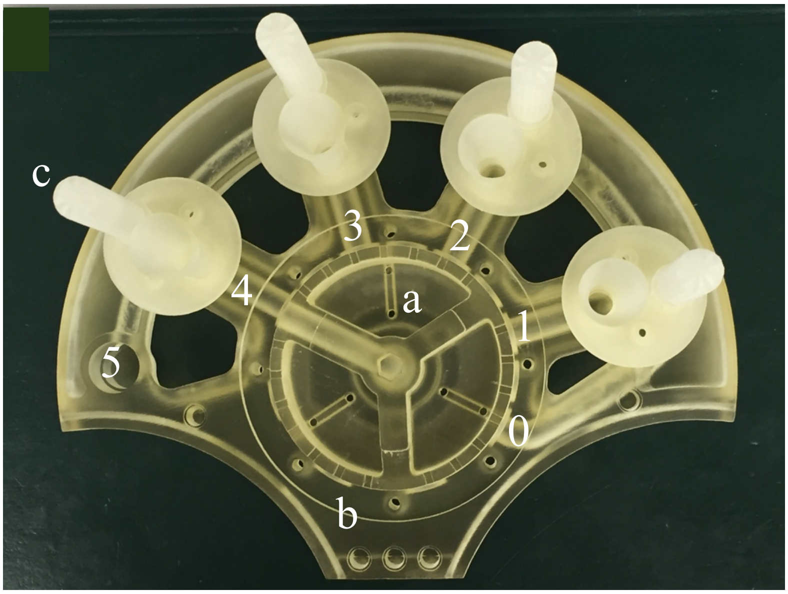

Figure A2: Sampler elements: (a) sample selector rotator; (b) main structural element of the sampler. Flow paths (1-4) direct water and particles into sample bottles or (0) to bypass sample bottles; and (c) particle retention system which bridges inflow channels and common exhaust manifold channel (5). Sample rotator is shown open at position 4. When not sampling, the rotator is sealed to closed positions.

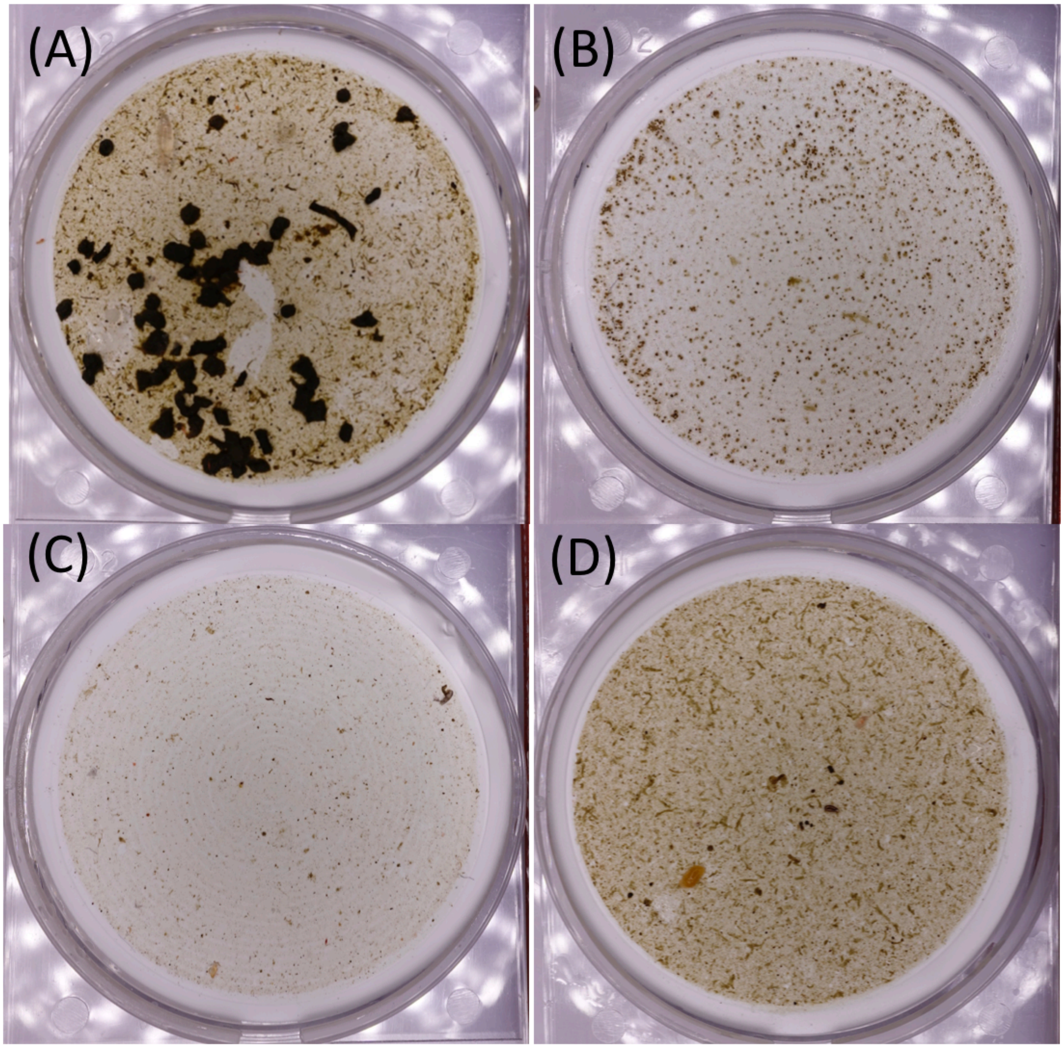

Figure A3: Representative images of sampled particulates from locations 1-4. The process of sampling retains morphology of cohesive aggregates and. Turbulence on transit from imaging stage to bottle does disrupt the integrity of loosely aggregated millimeter sized particles such as represented in Figure 3D. (a) Location 1. CFE 002 dive 42 - Days 160.623 to 160.791 - Depth 119.4 ± 7.8 m. (b) Location 2. CFE 004 dive 71 - Days 167.034 to 167.202 - Depth 157.6 ± 3.4 m. (c) CFE 002 dive 90 – Days 171.190 171.369 - Depth 126.9 ± 4.8 m. (d). Location 4. CFE 002 dive 101 - Days 174.479 to 174.646 - Depth 139.9 ± 3.0 m. 5